



Flame Dynamics Modelling Using Artificially Thickened Models

Omer Rathore¹ · Salvador Navarro-Martinez¹

Received: 21 January 2023 / Accepted: 31 May 2023
© The Author(s) 2023

Abstract

Thickened flame models are prolific in the literature and offer an effective method of resolving flame dynamics on coarse LES meshes. The current state of the art relies heavily on the use of efficiency functions to compensate for impaired wrinkling of the thickened flame. However in practice these functions can involve parameters that are difficult to determine, perform poorly outside of certain ranges or require a posteriori analysis to evaluate performance. An alternative based on a generalised thickening is evaluated across a range of canonical configurations. The approach is demonstrated to perform well across a large range of thickening factors in capturing phenomena such as localised quenching and pinch off as well as generation of flame surface. Including good performance even in the case of large flame dynamics under acoustic forcing where the model has a clear advantage over DNS in achieving grid independence. Finally the approach is unified into an Large Eddy Simulation/Adaptive Mesh Refinement framework and applied to a turbulent Bunsen flame. The results show that even if the internal flame structure is poorly resolved on the original mesh, the global system behaviour is well predicted and compares favourably with other approaches.

Keywords LES · ATF · Flame dynamics · Premixed flames

1 Introduction

Large Eddy Simulation (LES) provides an attractive solution to model turbulent reactive flows. LES mitigates the prohibitive computational cost of Direct Numerical Simulations, by limiting the resolved range of turbulence to the larger energy containing scales and filtering out smaller ones. Albeit straightforward in principle, many open questions remain (Pope 2004), with the main difficulty stemming from having to replace filtered scales with appropriate models that often still remain elusive. Turbulent combustion poses additional

✉ Salvador Navarro-Martinez
s.navarro@imperial.ac.uk

Omer Rathore
o.rathore@imperial.ac.uk

¹ Department Mechanical Engineering, Imperial College London, Exhibition Road, London SW7 2AZ, UK

challenges, for example at high Reynolds and Damköhler numbers, the dominant rate controlling processes of molecular mixing and chemical reactions occur below the filter width (Peters 2001). Hence a complex and non-linear turbulence-chemistry interaction must be accounted for at the filtered level. A large selection of models have been developed over the years with their respective advantages and disadvantages (Pitsch 2006; Fureby 2009) along with a diligent framework to determine quality metrics and meshing guidelines (Freitag and Klein 2006; Geurts and Fröhlich 2002; Chow and Moin 2003). Notable LES models in premixed combustion include solving a G-equation Pitsch and Duchamp de Lageneste (2002), the application of Flame Surface Density (FSD) models from Hawkes and Cant (2000), Flamelet Generated Manifold method Van Oijen and De Goey (2000) and the Presumed Conditional Moment-FPI approach of Domingo et al. (2005).

The focus in this paper will be on a particular class of turbulent combustion methods named Artificially Thickened Flame (ATF) models, also known as Thickened Flame Model (TFM). The use of ATF models is widespread in literature and has been applied in a variety of configurations, including gas turbine combustors (Gicquel et al. 2012), stratified combustion (Kazmouz et al. 2022), and even non-premixed flames (Cuenot et al. 2022) and Deflagration to Detonation Transition (Emami et al. 2015), among others. In a very recent comparative study (Kuhlmann et al. 2022), ATF was seen to perform better than a common LES alternative (FSD model) in predicting flame dynamics. ATF basically works by 'thickening' the flame, so the mesh can resolve the scalar gradients across the flame. This has a dual effect, it allows to capture the flame dynamics and secondly, it minimises the numerical diffusion errors associated with resolving the sharp jumps of the scalar across the flame.

However, ATF models are limited by the use of an efficiency function. This function controls how turbulence affects the flame dynamics. It can be considered somehow analogous as the problem of modelling sub-grid flame wrinkling in Flame Surface Density Models. This is an unsolved problem that conditions the applicability of ATF models. This paper examines the applicability of ATF models in flames that have strong dynamics and interact strongly with the flow. A modified ATF model is proposed to produce a dynamic formulation that does not require an efficiency function, is easy to implement and improves the description of flame-turbulence interaction. The method does not depend on tuning parameters other than the thickening factor. As such it has a wide range of applicability and can easily be coupled with other LES methods for a hybrid approach. The paper is structured as follows. First, the classical ATF model is described together with the proposed modification. Then the models are compared in a series of vortex-flame interactions, acoustically forced flames and finally in a turbulent Bunsen burner.

2 Mathematical Background

2.1 Conventional ATF

The ATF model was first proposed by Butler and O'Rourke (1977) and subsequently applied to the LES of combustion instabilities by Thibaut and Candel (1998). Motivation for the approach stems from the fact that the flame front is usually too thin to be resolved on a typical LES mesh, and instead simply perceived as a region of sharp discontinuity. The method is a spatial and temporal transformation of the flame from a course mesh (x_i, t) to a finer mesh (ξ_i, τ) . The aim is to provide adequate resolution within the flame front (i.e.

region of sharpest gradients) on the transformed mesh despite having insufficient resolution on the coarse LES mesh. The geometry transformation ratio, \mathcal{F} , is called the thickening factor. In the original work the thickening factor was independent of spatial coordinate, leading to $\xi_i = \mathcal{F}x_i$ and $\tau = \mathcal{F}t$. Conventionally (Colin et al. 2000; De and Acharya 2009) the transformation is applied to the species transport equation only:

$$\frac{\partial \rho Y_k}{\partial \tau} + \frac{\partial \rho u_i Y_k}{\partial \xi_i} = \frac{\partial}{\partial \xi_i} \left(\rho D \mathcal{F} \frac{\partial Y_k}{\partial \xi_i} \right) + \frac{\dot{\omega}}{\mathcal{F}} \tag{1}$$

The flame speed and thickness following laminar premixed flame theory (Kuo 1986; Williams 2018), are respectively:

$$s_l^0 \propto \sqrt{D \dot{\omega}} \quad \text{and} \quad \delta^0 \propto D/s_l^0 \tag{2}$$

and their respective transformed quantities, denoted by $\hat{\cdot}$, are

$$\hat{s}_l^0 \propto \sqrt{D \mathcal{F} (\dot{\omega} / \mathcal{F})} \quad \text{and} \quad \hat{\delta}^0 \propto \mathcal{F} D / \hat{s}_l^0 \tag{3}$$

The transformation ‘‘thickens’’ the flame but maintains the correct flame speed by increasing diffusion accordingly. If the grid is able to capture the flame zone accurately with the appropriate \mathcal{F} then inside the thickened region the flame is equivalent to the unfiltered, fully resolved flame. This is promising as it suggests there is no need for SGS modelling of the filtered source term. However DNS of flame/vortex interaction (Poinsot et al. 1991) demonstrated that the thickened flame responds differently to turbulence. Even if the transformation preserves laminar flame speed the same is not true for the Damköhler number which represents the ratio between characteristic turbulent and chemical time scales:

$$\text{Da} = \frac{\tau_t}{\tau_c} = \frac{l_t}{u'} \frac{s_l^0}{\delta^0} \tag{4}$$

For the thickened flame the characteristic size of turbulent motions (l_t) remains unchanged while the flame thickness is \mathcal{F} times bigger, leading to a reduction of Damköhler number by the same thickening factor. As a result the flame becomes increasingly insensitive to turbulence where vortices smaller than $\mathcal{F} \delta_f^0$ are no longer able to interact with the flame (Poinsot et al. 1991; Colin et al. 2000). This can be graphically interpreted as removing the SGS flame wrinkling as seen in Fig. 1 below.

The sub-grid wrinkling requires modelling and this is usually done in the ATF context by the inclusion of a so called *efficiency function* Colin et al. (2000); Charlette et al. (2002). The efficiency function, E , is defined by a dimensionless wrinkling factor \mathcal{E} , and its ratio between a laminar flame compared with its thickened counterpart. Inclusion into the ATF model results in a modification to the reactive scalar transport equation:

$$\frac{\partial \rho Y_k}{\partial \tau} + \frac{\partial \rho u_i Y_k}{\partial \xi_i} = \frac{\partial}{\partial \xi_i} \left(\rho D E \mathcal{F} \frac{\partial Y_k}{\partial \xi_i} \right) + \frac{E \dot{\omega}}{\mathcal{F}} \tag{5}$$

$$E = \frac{\mathcal{E}|_{\delta_f = \hat{\delta}_f^0}}{\mathcal{E}|_{\delta_f = \delta_f^0}} \geq 1 \tag{6}$$

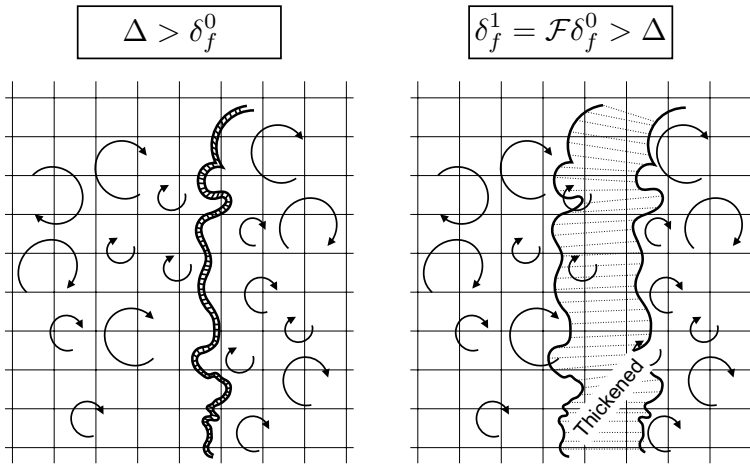


Fig. 1 Classical ATF. Only the flame is thickened while turbulence is unaffected by the transformation

The factor \mathcal{E} essentially relates the total flame front wrinkling with its resolved component. It can be approximated as:

$$\mathcal{E} \approx 1 + \beta \Delta | \langle \nabla \cdot \vec{n} \rangle_{sgs} | \quad (7)$$

where β is a constant and $| \langle \nabla \cdot \vec{n} \rangle_{sgs} |$ is the SGS surface curvature. Colin et al. (2000) proposed a model, assuming equilibrium between SGS flame surface and turbulence, that relates SGS curvature to the straining rate which is then approximated by a fitting function, Γ , to agree with DNS data of flame-vortex interaction. The resulting expression is:

$$\mathcal{E} = 1 + \beta \frac{u'_{\Delta}}{s_l^0} \Gamma \left(\frac{\Delta}{\delta_f^0}, \frac{u'_{\Delta}}{s_l^0} \right) \quad (8)$$

where the fitting function depends on the filter width to flame thickness and turbulent SGS velocity fluctuation (u'_{Δ}) to flame speed ratios. This formulation has been revisited over the years, for example by Charlette et al. (2002) who suggested a power law model which relates flame surface area to a characteristic cut-off scale, or by De and Acharya (2009) who suggest modifications to the fitting parameter to allow for better agreement with DNS.

Despite these improvements the model remains reliant on several assumptions, most notably perhaps on approximations used to find SGS quantities needed as inputs. Evaluation of u'_{Δ} is not trivial. Colin et al. (2000) proposed the expression used in many subsequent models (including Charlette et al. (2002)):

$$u'_{\Delta} = C_2 \Delta^3 | \nabla^2 (\nabla \times \vec{u}) | \quad (9)$$

and argued that this expression is independent of heat release. However, vorticity transport is known to be affected by heat release (Louch and Bray 2001; McMurtry et al. 1986, 1989) it is likely there will be some effect passed onto expression (9) via changes in the resolved vorticity field, i.e. $(\nabla \times \vec{u})$.

Moreover difficulties remain in determining the many empirical constants used in finding the efficiency function as well as their application outside of already validated regimes.

Although work has been done to automate this process with dynamic evaluation (Rochette et al. 2018) or eliminating the dependency on a SGS velocity fluctuation (Wang et al. 2011), most implementations rely on user defined parameters. The effects of choice of constants and method of parameter evaluation remains unclear and often necessitates a posteriori assessment in realistic engineering configurations (De and Acharya 2009).

Since it's original conception, the ATF model has been extended to include the use of a sensor to apply the transformation in the local region of the flame only (Légier et al. 2002). For perfectly premixed flames the differences are expected to be small since the model only has significant effects in regions where there are gradients in the scalar field i.e. inside the reaction zone. However the use of flame sensors (Durand and Polifke 2007) has allowed application to more general cases such as non-perfectly premixed flames, while preserving mixing processes outside of the flame.

Despite theoretical shortcomings, the ATF model and its variants have been applied successfully in various LES configurations (Kuenne et al. 2011; Vermorel et al. 2017; Kraus et al. 2018). Good practice is to maintain $\delta^0/\Delta \geq 7$ (Rochette et al. 2018), and use moderate thickening factors $\mathcal{F} \leq 10$ (Kuenne et al. 2011; Popp et al. 2019).

Note that ATF models can respond differently in time since the equations are solved with respect to thickened time, τ , instead of t , so care needs to be taken for configurations that involve large transients (Charlette et al. 2002). Despite its success, applications of the ATF model to systems where the flame has large dynamics are rare. Auzillon et al. (2011) showed that in acoustically forced quasi-laminar flames, the thickening approach strongly affects the flame dynamics. Similarly, strained flames using the ATF model predict lower consumption speeds (Popp et al. 2019).

2.2 Modified ATF

The proposed model applies the geometric transformation to all of the governing transport equations instead of just the reactive scalars. The idea is that by “thickening” *all scales*, including the turbulent integral scale, flame/turbulence interaction is better preserved as reflected by the Damköhler number:

$$\widehat{Da} = \frac{\hat{\lambda}_t s_l^0}{u' \delta_f^0} = \frac{\mathcal{F} \lambda_t s_l^0}{u' \mathcal{F} \delta_f^0} = Da \quad (10)$$

where the thickened Damköhler number remains unchanged even without the inclusion of an efficiency function. Theoretically with a large enough thickening factor it would be possible to preserve Karlovitz numbers as well since Kolmogorov scales would also “thicken”. However in large-scale simulations this may be impractical if the filter width is much larger than Kolmogorov scales.

The transformation is kept local in the region of the flame via the use of a flame sensor, Ω . The sensor helps to limit effects on transient response of the system since as compared with before all the equations are now with respect to thickened time and not just the species transport equation. There is a stark contrast when comparing the modified and classical ATF, in that the absence of a sensor with the proposed methodology is meaningless as it equates to scaling the entire domain. The challenge is to blend the two sub-domains into the same simulation, one thickened and one not. To this end the sensor is critical and behaves in the same manner as shock-detectors in shock/turbulent simulations (Ducros et al. 1999; Pirozzoli 2011), where the shock is numerically thickened by an artificial viscosity, either

explicitly or implicitly by the numerical scheme. Figure 2 illustrates this new approach which simultaneously transforms both flame and turbulent scales.

To derive the corresponding set of equations consider a generic thickening factor that now depends on position, the coordinate transformation, from $(x, y) \rightarrow (\zeta, \eta)$ is represented by:

$$d\zeta = \frac{\partial \zeta}{\partial x} dx + \frac{\partial \zeta}{\partial y} dy \quad (11)$$

$$d\eta = \frac{\partial \eta}{\partial x} dx + \frac{\partial \eta}{\partial y} dy \quad (12)$$

$$\frac{\partial \zeta}{\partial x} = \frac{\partial \eta}{\partial y} = \mathcal{F} \quad (13)$$

and

$$\frac{\partial \eta}{\partial x} = \frac{\partial \zeta}{\partial y} = 0 \quad (14)$$

where $\mathcal{F} = \mathcal{F}(x, y)$. Using chain rule, the derivative of an arbitrary scalar, ϕ , is

$$\frac{\partial \phi}{\partial x} = \frac{\partial \phi}{\partial \zeta} \frac{\partial \zeta}{\partial x} = \frac{\partial \phi}{\partial \zeta} \mathcal{F} \quad (15)$$

similarly

$$\frac{\partial \phi}{\partial y} = \frac{\partial \phi}{\partial \eta} \mathcal{F} \quad (16)$$

The convective term is then:

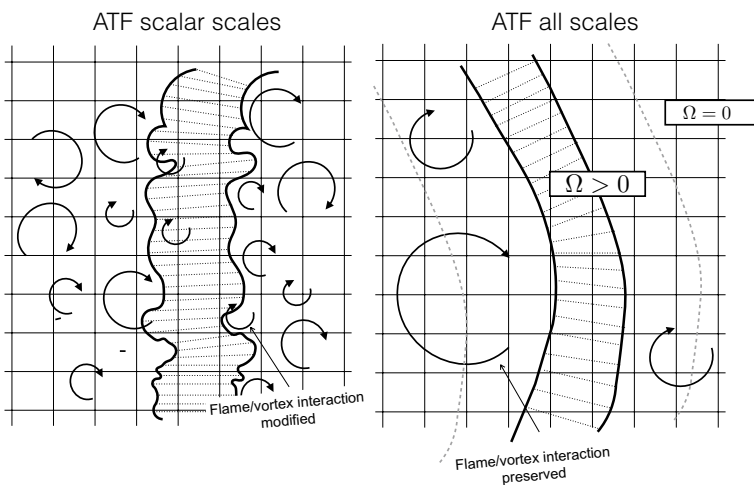


Fig. 2 Modified ATF model. By thickening turbulent scales as well it preserves flame/turbulence interaction within the reaction zone ($\Omega > 0$)

$$\frac{\partial \rho u \phi}{\partial x} = \frac{\partial \rho u \phi}{\partial \zeta} \mathcal{F} \tag{17}$$

and the diffusive term:

$$\frac{\partial}{\partial x} \left[D \frac{\partial \phi}{\partial x} \right] = \frac{\partial}{\partial \zeta} \left[D \frac{\partial \phi}{\partial x} \right] \mathcal{F} = \frac{\partial}{\partial \zeta} \left[D \mathcal{F} \frac{\partial \phi}{\partial \zeta} \right] \mathcal{F} = \mathcal{F} \frac{\partial}{\partial \zeta} \left[\underbrace{D \mathcal{F}}_{D^*} \frac{\partial \phi}{\partial \zeta} \right] \tag{18}$$

Replacing in a convection-diffusion equation, with $\xi_i = (\zeta, \eta)$:

$$\frac{\partial \rho \phi}{\partial t} + \mathcal{F} \frac{\partial \rho u_i \phi}{\partial \xi_i} = \mathcal{F} \frac{\partial}{\partial \xi_i} \left[D \mathcal{F} \frac{\partial \phi}{\partial \xi_i} \right] + \dot{\omega} \tag{19}$$

Note at this point that length scales have been transformed from $x_i \rightarrow \xi_i$. In order to preserve velocities, and eventually Reynolds number, it is necessary to transform time as well. The temporal term:

$$\frac{\partial \phi}{\partial t} = \frac{\partial \phi}{\partial \tau} \frac{\partial \tau}{\partial t} = \frac{\partial \phi}{\partial \tau} \mathcal{F} \tag{20}$$

Replacing into the convection-diffusion equation:

$$\frac{\partial \rho \phi}{\partial \tau} \mathcal{F} + \mathcal{F} \frac{\partial \rho u_i \phi}{\partial \xi_i} = \mathcal{F} \frac{\partial}{\partial \xi_i} \left[D \mathcal{F} \frac{\partial \phi}{\partial \xi_i} \right] + \dot{\omega} \tag{21}$$

Dividing through by \mathcal{F} :

$$\frac{\partial \rho \phi}{\partial \tau} + \frac{\partial \rho u_i \phi}{\partial \xi_i} = \frac{\partial}{\partial \xi_i} \left[D \mathcal{F} \frac{\partial \phi}{\partial \xi_i} \right] + \frac{\dot{\omega}}{\mathcal{F}} \tag{22}$$

$$\frac{\partial \xi_i}{\partial x_i} = \frac{\partial \tau}{\partial t} = \mathcal{F}(x_i) \tag{23}$$

The above transformation is now applied to the full set of conservation equations to give:

$$\frac{\partial \bar{\rho}}{\partial \tau} + \frac{\partial \bar{\rho} \tilde{u}_i}{\partial \xi_i} = 0 \tag{24}$$

$$\frac{\partial \bar{\rho} \tilde{u}_i}{\partial \tau} + \frac{\partial \bar{\rho} \tilde{u}_i \tilde{u}_j}{\partial \xi_i} + \frac{\partial \bar{p}}{\partial \xi_i} = \frac{\partial 2 \mathcal{F} \mu \tilde{S}_{ij}^*}{\partial \xi_i} - (1 - \Omega) \frac{\partial \tau_{ij}^{sgs}}{\partial \xi_j} \tag{25}$$

$$\frac{\partial \bar{\rho} \tilde{e}}{\partial \tau} + \frac{\partial (\bar{\rho} \tilde{e} + \bar{\rho}) \tilde{u}_i}{\partial \xi_i} = \frac{\partial \bar{q}_i}{\partial \xi_i} + \frac{\partial 2 \mathcal{F} \mu \tilde{S}_{ij}^* \tilde{u}_j}{\partial \xi_i} + (1 - \Omega) \frac{\partial}{\partial \xi_j} (H_i^{sgs} + \sigma^{sgs}) \tag{26}$$

$$\frac{\partial \bar{\rho} \tilde{Y}_k}{\partial \tau} + \frac{\partial \bar{\rho} \tilde{u}_i \tilde{Y}_k}{\partial \xi_i} = \frac{\partial}{\partial \xi_i} \left(\bar{\rho} \mathcal{F} D \frac{\partial \tilde{Y}_k}{\partial \xi_i} \right) + \frac{\bar{\rho} \dot{\omega}}{\mathcal{F}} - (1 - \Omega) \frac{\partial J_i^{sgs}}{\partial \xi_j} \tag{27}$$

where $S_{ij}^* = S_{ij} - \delta_{ij}S_{kk}/3$ and SGS turbulent transport models have been turned off in the vicinity of the flame by the $(1 - \Omega)$ term which is approximately zero in this neighbourhood. This avoids an artificial increase to diffusivity and subsequently flame speed (De and Acharya 2009) while maintaining $\tilde{\phi} \rightarrow \phi$ in the reactive zone.

Previous research endeavours have also experimented with thickening alternative equations to just those of reactive scalar transport. Notable examples include Picciani et al. (2018a, 2018b) who apply a thickening transformation to the stochastic fields equations or Yu and Navarro-Martinez (2015) who employ a more generalised thickening in the context of DDT. To the authors' knowledge this work forms the first thorough validation, evaluation and subsequent application to a variety of subsonic premixed flames with the modified ATF model described above. This is in conjunction with the novel dynamic formulation described next.

2.3 Dynamic Formulation

The thickening factor used above in Eqs. (24)–(27) is expanded to give its dynamic form as

$$\mathcal{F} = 1 + (\mathcal{F}_0 - 1)\Omega \quad (28)$$

where \mathcal{F}_0 is a user defined function of mesh spacing that determines the desired number of points within the flame. Meanwhile the spatial dependence is incorporated into the flame sensor, Ω , usually by conditioning on progress variable. Several options are available in literature that range in complexity from static definitions (Proch and Kempf 2014) to self adapting methods (Rochette et al. 2020) as well as various optimisations dependent on equivalence ratio regime (Zhang et al. 2021). For the cases considered here which are limited to premixed flames close to stoichiometric conditions, static sensors are shown to be sufficient and simple to implement. The commonly used implementation of Durand and Polifke (2007) is given by Eq. (29), note that here the progress variable is normalised on fuel mass fraction to be zero in the fresh region and unity in the burnt.

$$\Omega = 16[c(1 - c)]^2 \quad (29)$$

Modest improvement was observed when using a new flame sensor correlated on a regression of the heat release distribution from a 1D flame onto progress variable. This was done by conducting DNS of a 1D stable flame before extracting the heat release rate conditioned on progress variable and fitting a polynomial to the data. The resulting expression for methane flames used here is given by the fifth order polynomial:

$$\Omega = -0.006 + 0.488c - 7.729c^2 + 46.365c^3 - 67.638c^4 + 28.473c^5 \quad (30)$$

The specific value of coefficients in the above expression are naturally subject to change when using a different chemistry scheme, or pressure or equivalence ratio, as the profile of heat release in progress variable space will be somewhat different. The overhead of the sensor calculation is very small since it relies on a priori one dimensional flame simulation. The key result from the proposed methodology is the generation of sensors that are asymmetric in nature as seen in Fig. 3.

Since the reactions occurring at higher progress variable (i.e. closer to the burnt side) are at higher temperature and release more energy, it is argued that this region requires the most thickening to resolve the nonlinear flame dynamics. Indeed the notion of a flame sensor peaking at a progress variable of 0.5 originates more from numerical motivations

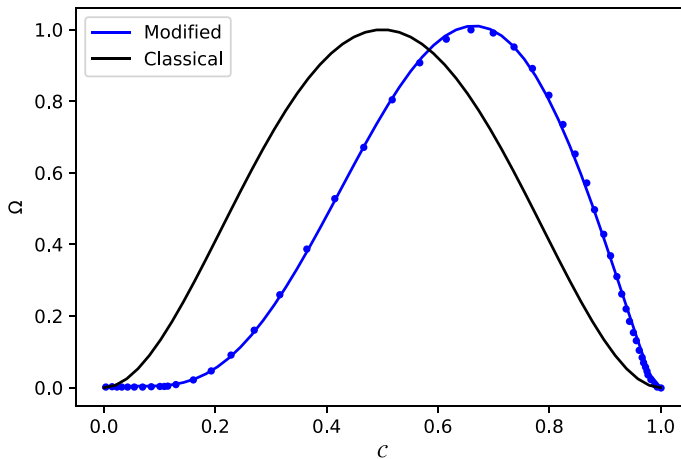


Fig. 3 Structure of the hitherto termed “classical” flame sensor of Durand and Polifke (2007) and the proposed asymmetric modification for which both regression data points and polynomial fit are displayed

than any particular physical justification. In alternative definitions of the progress variable, using element mass fraction for intermediates, this sensor functional dependence may be different. Furthermore, from a more practical standpoint, many modern combustion codes include a cutoff temperature for calculating chemical kinetics. This is a purely empirical “minimum activation temperature” designed to increase computational efficiency by restricting the number of points that enter chemical subroutines. The asymmetric sensor inherently accommodates this by limiting thickening close to zero on the lower temperature, fresh side thus avoiding an artificial increase in diffusivity in regions where the chemistry is numerically turned off. The sensor’s localized transformation limits how well the flow dynamics are preserved in the transition region. This applies to all types of ATF models, both the classical and the version proposed here. When the heat release is spread over a large flame area, it reduces thermal expansion, which in turn affects the flow field. However, the impact of MATF is smaller than the CATF as Damköhler number is preserved and the maximum thickening occurs in a very thin region within the center of the flame as determined by the sensor. For progress variables outside the 0.1–0.9 range, the sensor value will be very small and introduce a modest modification of the flow field and therefore impact of incoming vortices. This thickening would be smaller than the “numerical thickening” associated with numerical schemes in the neighbourhood of the flame. Nevertheless, the choice of sensor will impact flame dynamics and a-priori is difficult to suggest an optimal choice which may depend on flow/conditions and computational complexity.

2.4 Flow Solver

All simulations were carried out using an in-house, finite-difference, compressible, density based flow solver named CompReal Almeida and Navarro-Martinez (2019). Spatial discretisation is implemented using a fourth order skew-symmetric, conservative formulation Ducros et al. (2000), along with high order explicit Runge–Kutta time marching. Hydrogen/air flames are modelled using a 19 step reduced reaction scheme Yetter et al. (1991) while methane/air reactions are accounted for using a 2 step, 5 species mechanism Franzelli et al. (2010). The domain boundaries employ NSCBC Poinso and Lele (1992)

methods with transverse corrections and relaxation parameters Lodato (2008). Two dimensional simulations presented here rely on regular Cartesian grids while the three dimensional Bunsen flame incorporated Adaptive Mesh Refinement (AMR) using the BoxLib library Bell et al. (2012).

3 Results

The proposed model was evaluated in a series of canonical configurations prior to application in a realistic fully turbulent Bunsen flame. Each test case was designed to assess known weaknesses of ATF methods. Starting with the flame-vortex interaction to assess the effect of thickening on flame-turbulence interaction in a controlled environment. Despite its apparent simplicity this configuration laid much of the framework for the original efficiency function based methods of (Colin et al. 2000; Charlette et al. 2002).

Next an axisymmetric flame undergoing acoustic excitation is examined in order to determine the effect of the thickening transformation on not just the reactive scalar but also momentum equations. The large transients make this a challenging case for any ATF methodology.

Finally the inherent advantages of the proposed approach to best leverage the advantages of AMR are demonstrated for a realistic turbulent flame. The filter width can be difficult to precisely determine in AMR simulations due to the nested grid levels. However the proposed approach only has an implicit dependence on SGS quantities and filtering is turned off in the region of the flame. Therefore it is well poised to take advantage of the resolution AMR grants without needing additional corrections as is the case when using as efficiency function Mehl et al. (2021). The same sensor is used in all ATF approaches unless stated otherwise.

3.1 Flame-Vortex Interaction

A common limitation of ATF models is difficulty in capturing turbulence induced flame wrinkling. This is evaluated for the proposed approach by simulating a pair of counter-rotating vortices upstream of an initially planar flame front and tracking the flame front during impact. The size and intensity of the vortex pair are based on earlier findings (Colin et al. 2000) and only the most challenging cases are shown here. The mesh resolution is kept sufficient to ensure at least 10 points within the laminar flame thickness, so that all relevant scales are resolved a priori, in order to isolate the effects of the thickening transformation. The inlet is perfectly premixed hydrogen/air at unity equivalence ratio and standard temperature/pressure.

The chosen vortex size is roughly of the order of laminar flame thickness i.e. smaller than vortices considered in Colin et al. (2000). Therefore in a thickened context the vortex will always see the flame as *thick*, hence placing the interaction somewhere between the cut-off (where vortices can no longer interact with the flame) and intermediate scales (where flame-vortex interaction is impaired) for which classical ATF fails. The vortex strength is characterised by the ratio of v'/s_l and kept low to evaluate impact of modelling assumptions on the smallest and weakest vortices. Three cases, corresponding to values of 1, 2 and 4, were simulated across a range of thickening factors.

Starting with the vortex strength of 4, a qualitative representation of the flame-vortex interaction and its evolution in time is displayed in Fig. 4. Generally speaking, the model

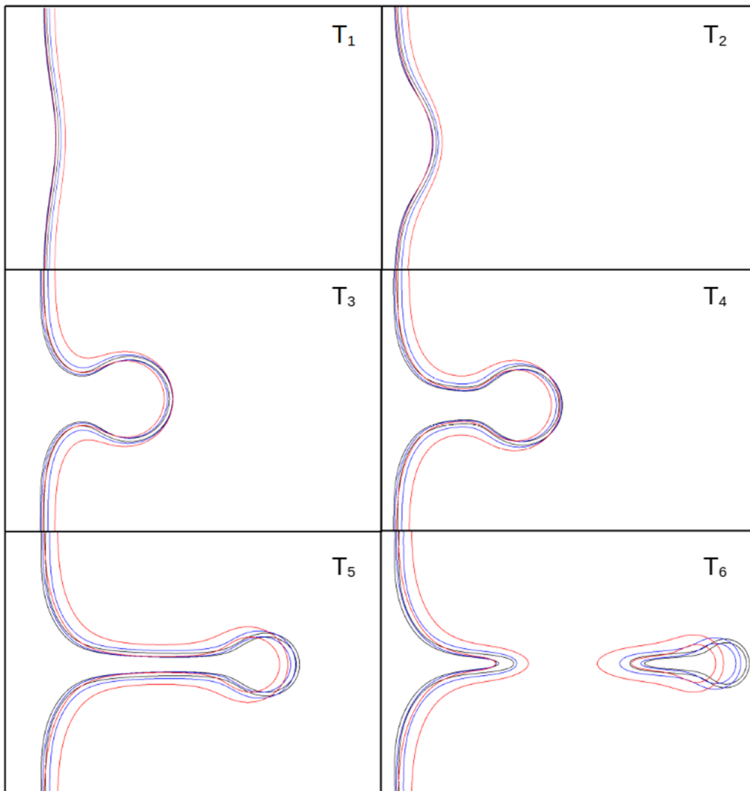


Fig. 4 Evolution of the progress variable iso-contours (0.1 and 0.9) during flame-vortex interaction for $v'/s_l = 4$. DNS (black), MATF with $\mathcal{F} = 2$ (blue) and $\mathcal{F} = 4$ (red)

captures the nature of the interaction very well across a wide range of phenomena ranging from initial wrinkling (top row) to neck formation (middle) and subsequent pinch-off/pocket formation (bottom) even without an efficiency function.

There are small differences with respect to the transient response. This is not surprising as ATF models solve with respect to *thickened time*. Despite this the use of an appropriate sensor to limit the transformation to the reaction zone does seem to have mitigated most of these inherent shortcomings. For the purposes of pinch-off, the “neck” region is slightly wider than DNS, and pinch-off is delayed. Nevertheless, the remainder of the base flame can be seen to recover for all cases following pinch-off with good agreement.

Figure 5 focuses on the discrepancies at the most challenging scales. The top row highlights the phenomena described earlier where the wider neck region brought about by thickening lead to a small delay in pinch off. Nevertheless the shape of the pocket is well preserved. As the pocket is consumed some of the finer details are lost (bottom row). Structures of the order of δ_f^0 may indeed be distorted or lost as two flame elements separated by a distance of about δ_f^0 may no longer be separated when transformed into thickened space. Despite this, the overall flame dynamics in vorticity controlled regions across challenging phenomena such as quenching and pocket formation are replicated with the proposed methodology.

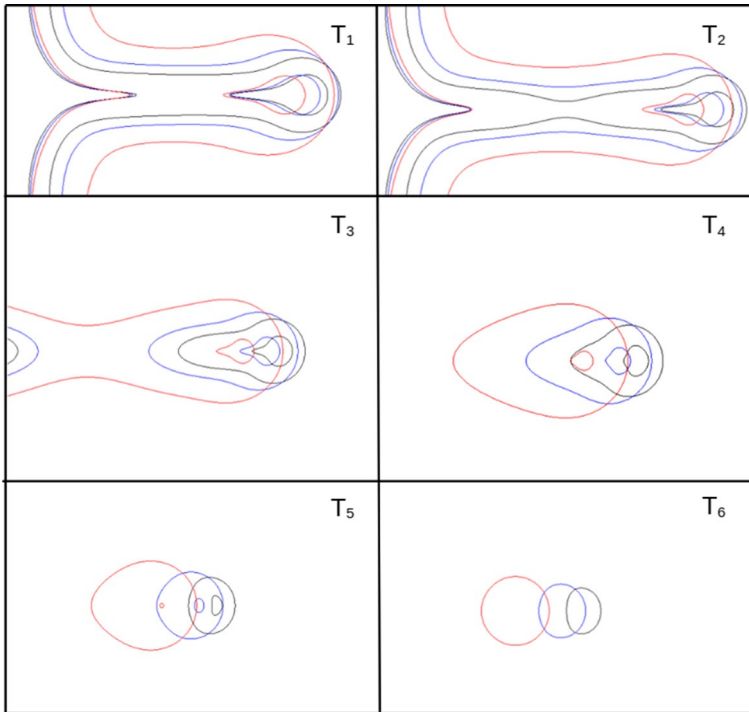


Fig. 5 Evolution of the progress variable iso-contours (0.1 and 0.9) during pocket formation and burnout for $v'/s_l = 4$. DNS (black), $\mathcal{F} = 2$ (blue) and $\mathcal{F} = 4$ (red)

Moreover the localised distortion has little effect on global system dynamics. Figure 6 displays the evolution of total heat release normalised to the undistorted/planar flame. For simple configurations, such as the flame single-vortex interaction, the net

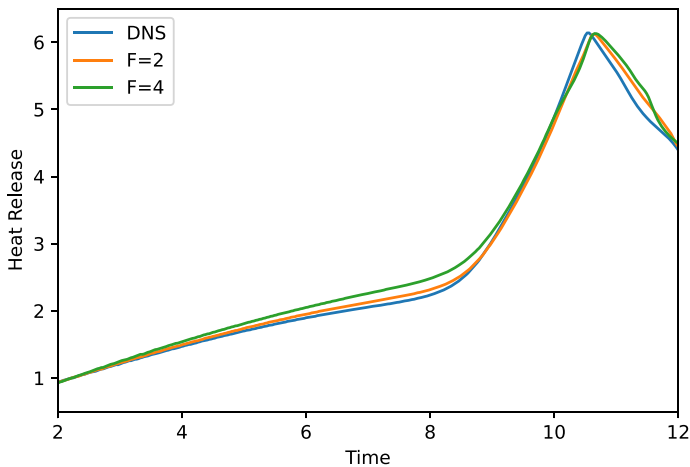


Fig. 6 Total non-dimensional heat release plotted against non-dimensional flame time

heat release rate can be considered as indicative of net flame surface area, hence consequentially representative of the effectiveness of a vortex at inducing flame wrinkling (Colin et al. 2000). The close agreement in peak heat release rate suggests that the methodology captures the overall effect of vortex induced flame wrinkling and its associated creation of flame surface.

The proposed approach is now tested across a larger range of thickening factors. Even if some of these values go beyond what is recommended for practical applications. Figure 7 illustrates the heat release evolution where the responses can be divided into two categories. Up to $\mathcal{F} = 10$ the peak heat release is captured well even if there are increasing differences in the transient buildup and subsequent annihilation of flame surface. This suggests good overall behaviour of the model in preserving the nature of flame response even under strain dominated behaviour. For values of the thickening factor greater than 15 there is a qualitative change in flame response, starting with the formation of a region resembling a plateau between times 10.5–11.1, directly after which the heat release continues to increase instead of falling.

Figure 8 displays a side by side comparison of progress variable distribution for DNS and $\mathcal{F} = 20$ in time increments of 0.3 from 10.5 to 11.1. The plateau in heat release at very large thickening therefore relates to the failure of entrained fresh mixture in completely pinching off and having an associated generation of flame surface. This is probably due to a complex interplay between delayed transient dynamics which are always difficult to preserve at such small scales due to the thickened time. The thickened space transformation can also displace flame contours which may affect the very small scales relevant for phenomena such as necking, pinch off, etc.

The unexpected increases in heat release can be an artifact of multi-step chemistry. Most of the ATF groundwork was laid using one-step chemistry (Colin et al. 2000; Charlette et al. 2002; Légier et al. 2002) with many practical implementations also adopting similarly simplified chemical kinetics (Strakey and Eggenpieler 2010; Hernández-Pérez et al. 2011; De and Acharya 2009). Few studies (Emami et al. 2015; Straub et al. 2018) incorporate detailed chemical schemes. With some recent works

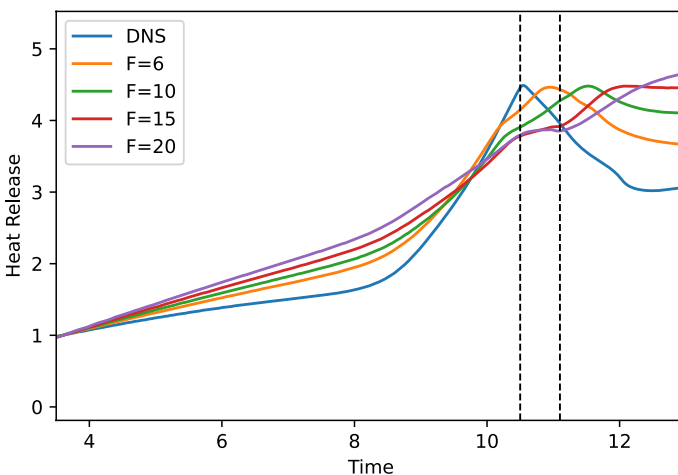


Fig. 7 Non-dimensional heat release against non-dimensional flame time. Dotted black lines encompass the region of time 10.5–11.1

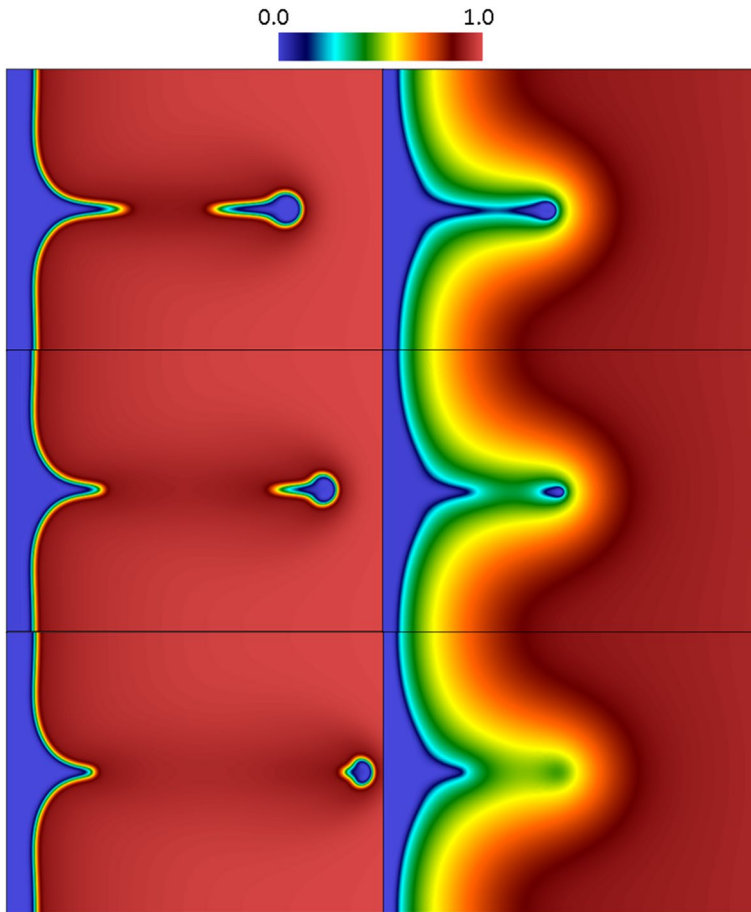


Fig. 8 Evolution of progress variable distribution through times 10.5–11.1 (top to bottom) for DNS (left) and $\mathcal{F} = 20$ (right)

(Maio et al. 2019; Bénard et al. 2019) beginning to attribute over predictions in intermediate species to the thickening transformation.

In the very non-linear flame reaction region, reactions peak at different values in progress variable space and are usually inter-dependant. Therefore applying a broadband thickening at large values does not necessarily conserve the nature of this inter-dependence, and as a result could influence global system parameters such as net reaction rate/heat release.

This is illustrated in Fig. 9 where the net reaction rate for selected species is compared between DNS and $\mathcal{F} = 15$. Some of the trajectories for other short lived radicals overshoot while others undershoot when compared with DNS. Essentially the global balance which is highly inter-dependant is not preserved as thickening does not affect all reactions equally. For practical systems where the complex balance between endo/exo-thermic reactions can determine the nature of local heat release and possible even system stability this warrants caution. However, these effects seem to be significant only at large thickening factors.

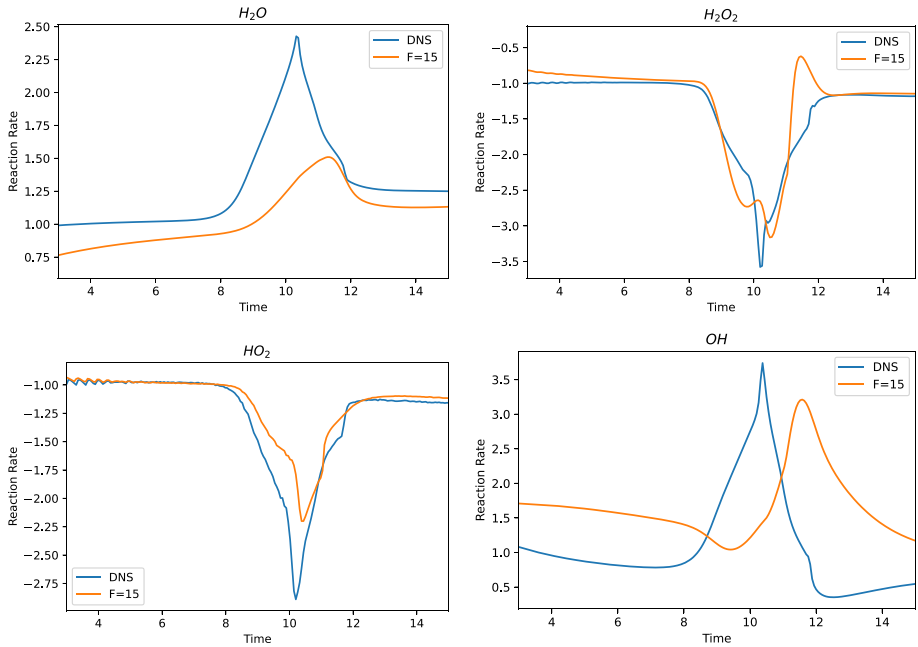


Fig. 9 Non-dimensional reaction rates for $\mathcal{F} = 15$ compared with DNS

Figure 10 highlights the benefits of the novel sensor that was proposed as part of this work when compared to the implementation of Durand and Polifke (2007), hitherto referred to as the “classical” sensor at moderate thickening. The peak heat release is captured well, suggestive of improved resolution of flame surface as well as potentially better conservation of complex chemistry effects. Meanwhile the classical sensor exhibits a small loss in peak heat release indicative of some detriment in capturing the finest scales.

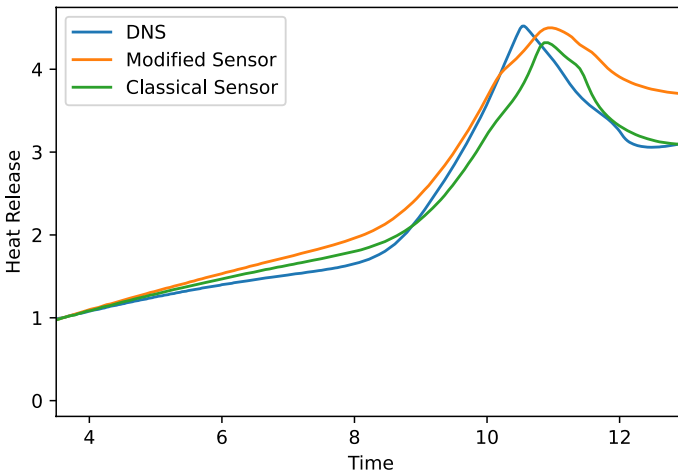


Fig. 10 Evolution of heat release for DNS and two sensor implementations coupled with $\mathcal{F} = 6$

Figure 11 displays results where the vortex intensity is decreased to 2 (same vortex size). Both CATF (thickening species only) and MATF (thickening all equations) solutions follow DNS with relatively decent agreement throughout the necking phase despite considerable thickening. A qualitative difference manifests in the final stages, where the DNS and proposed ATF model both result in localised quenching leading to pocket formation but CATF fails to do so.

A further reduction in strength leads Fig. 12, where the structure is now too weak to induce quenching. A pocket is no longer formed with localised wrinkling leading to entrainment of fresh mixture in the vortex trail instead. The proposed model follows DNS relatively well in the early stages but does not capture the finer details of the entrained profile.

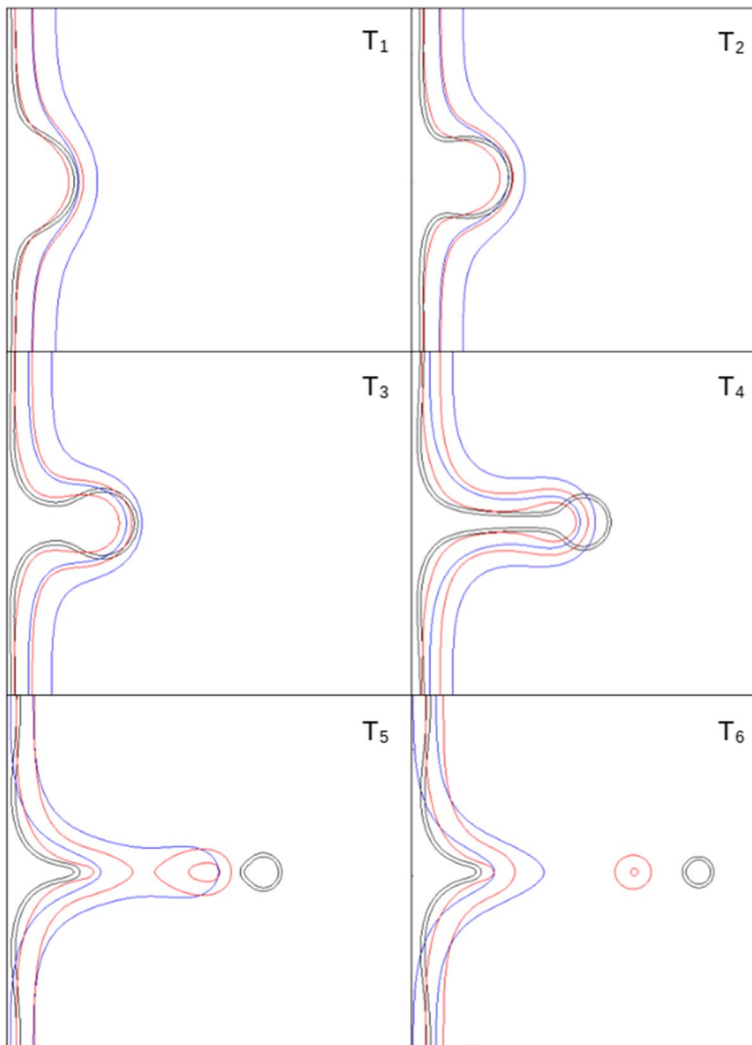


Fig. 11 Progress variable iso-contours (0.1–0.9) for $v'/s_l = 2$, shown for DNS (black) and CATF (blue)/MATF (red) with a thickening factor of 6

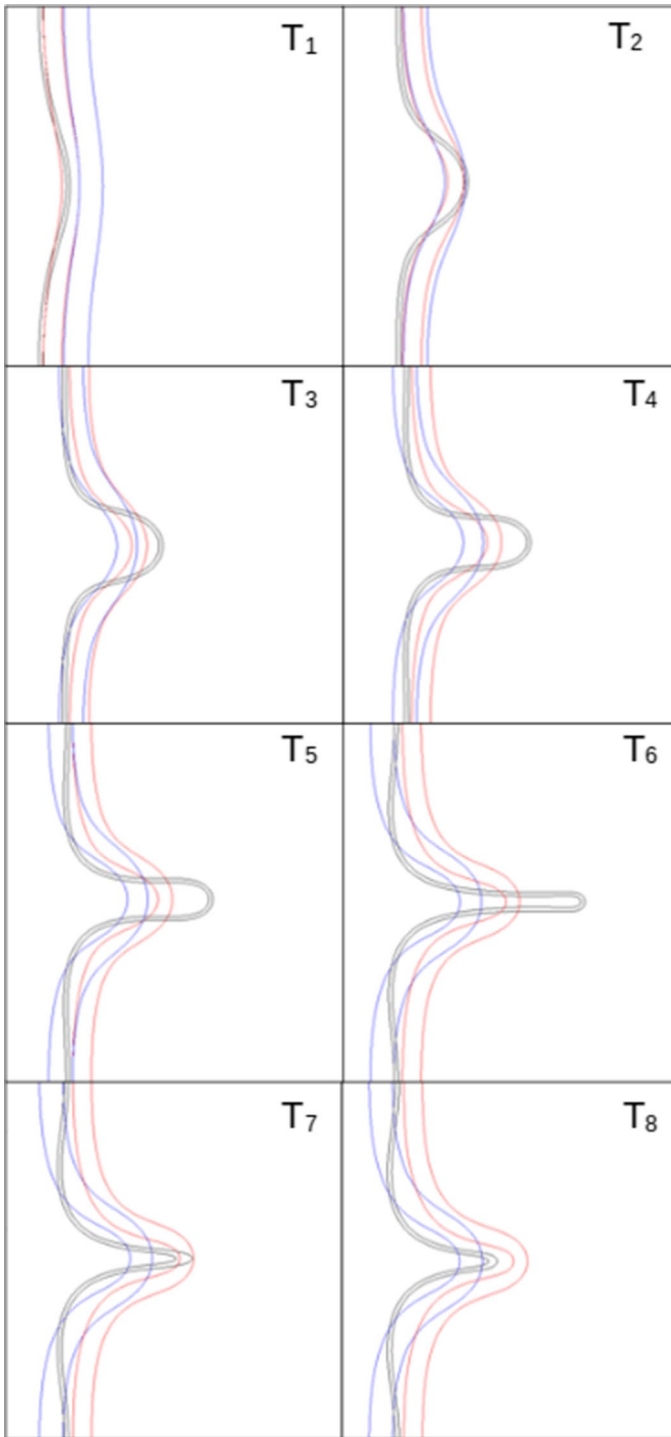


Fig. 12 Progress variable iso-contours (0.1–0.9) for $v'/s_l = 1$, shown for DNS (black) and CATF (blue)/MATF(red) with a thickening factor of 6

The flame response is inherently unsteady and depends on the transient variations of stretch coinciding with the vortex state at that particular times. As such, differences between specific instantaneous states identified during fast and unsteady processes are not surprising. The behaviour of the flame front seems to be better for the modified approach compared with CATF, suggesting potential advantages of the approach even for very weak structures that traditionally would require efficiency corrections.

3.2 Acoustically Modulated Flames

Durox et al. (2005, 2009) from their studies spanning various laminar premixed flame configurations, point out the crucial importance of accurately capturing the oscillating flow field (including motion in the shear layer) in order to reproduce reasonable flame response. Therefore this case evaluates the model across a much wider blend of facets which include disturbance formation but also convection through an active shear layer, thus extending potential applications to advection dominated flows.

Figure 13 illustrates the employed configuration where a 22 mm exit diameter burner issues perfectly premixed methane-air mixture at an equivalence ratio of 1.05, corresponding to a laminar burning velocity of 0.39 m/s. The inlet flow velocity is harmonically modulated by

$$v = \bar{v} + \sqrt{2}v' \sin(2\pi ft) \quad (31)$$

Where the mean inflow velocity, \bar{v} , is taken to be 0.97 m/s, the inflow RMS, v' , set to 0.19 m/s and the frequency, f , to 62.5 Hz. This collection of parameters is essentially a two-dimensional simplification of the experiments by Ducruix et al. (2000); Schuller et al. (2002).

This case was selected as the objective for a numerical study (Auzillon et al. 2011) that compared the effectiveness of different LES models in capturing flame response. Among which was the classic ATF model which was shown to perform poorly even at relatively low thickening factors. The objective here is to evaluate the effects of

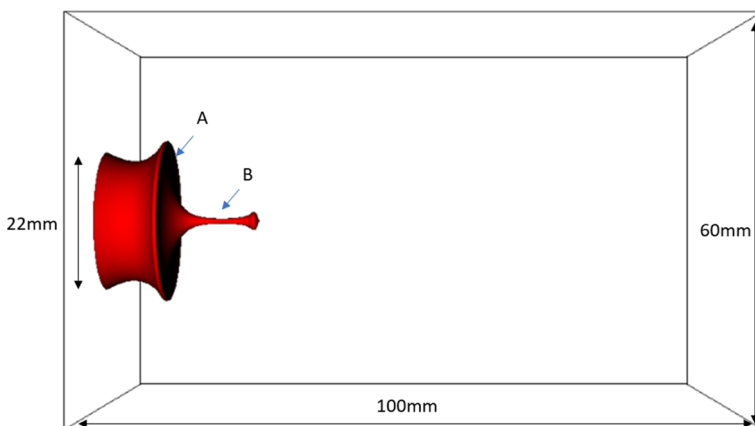


Fig. 13 General domain configuration with revolved flame solution showing cusping (A) and necking prior to pocket pinch off (B) during acoustic cycle

thickening on flame front dynamics and structure under the influence of acoustic loading. To limit uncertainties arising from SGS closures this is carried out in an environment where the flame is not wrinkled at the subgrid level i.e. all flow motions are fully resolved but the internal flame structure is not. Similarly, Auzillon et al. (2011) assume all SGS flow motions are resolved by the mesh in a bid to isolate effects of the thickening transformation itself.

Simulations were run for at least five forcing cycles after initial transients had passed, before data was sampled. This was done on two separate meshes, a finer mesh that was considered equivalent to DNS in order to isolate the effects of thickening only, and a coarser one to highlight the potential benefits of the proposed model. Relevant parameters in terms of points within the flame thickness for a thickening factor of 4 are presented in Table 1 where grid stretching was used to obtain the desired resolution.

Figure 14 shows instantaneous flame shapes throughout a single acoustic cycle for four different simulations. Namely DNS, the modified ATF approach (MATF) on two different meshes in accordance with Table 1 and no-model (NM) run on the course mesh which is representative of poorly resolved DNS. Most notable perhaps is the observation that MATF simulations exhibit strikingly similar behaviour at all times despite the differing mesh resolutions. This suggests a significant advantage in obtaining grid independent solutions much earlier than DNS, as evident by the discrepancies in NM.

All cases show disturbance formation at the base which then moves downstream along the flame front in the form of a convected wave, prior to tip instability. NM exhibits significant deviation from DNS even at the very start, as a consequence of delayed recovery from pinch off during the previous acoustic cycle. Meanwhile MATF shows relatively good agreement at the beginning, suggesting that even if there are some instantaneous differences due to temporal thickening, the overall periodic state of the system is preserved.

Figure 14 shows how the disturbance rolls up the flame sheet near the tip, causing break-away pockets of fresh mixture. Note how the next disturbance, which has only convected about a third of the way up the flame, still remains relatively in phase for all simulations.

The later stage of the cycle shows recovery from pinch off from the flame. The more dominant kinematic restoration effects negate small transient delays that arise during necking, as both DNS/MATF solutions come close to realigning. NM however exhibits impaired tip behaviour both in terms of time but also in the size of pocket formation which is significantly smaller.

A brief comparison with CATF at the same thickening factor of 4 is included in Fig. 15. Where CATF loses much of the finer details of the unsteady flame dynamics, particularly near the tip region. The overall response is relatively close to switching from a well defined convective mode where a disturbance progressively rolls up the entire length of the flame front to the more global, bulk oscillation mode as described in Auzillon et al. (2011). Flame shape in vicinity of the tip is not only flatter but also exhibits significant displacement, likely due to an inability of the classically thickened flame to fold in on itself or wrinkle in response to the same hydrodynamic driving force.

Table 1 Mesh resolution in near field of acoustically modulated flame simulations

| Description | $\approx \delta_f^0/\Delta$ | $\approx \delta_f^0/\Delta$ | Total points ($\times 10^6$) |
|-------------|-----------------------------|-----------------------------|--------------------------------|
| Fine | 8 | 30 | 4.3 |
| Coarse | 3 | 10 | 1.8 |

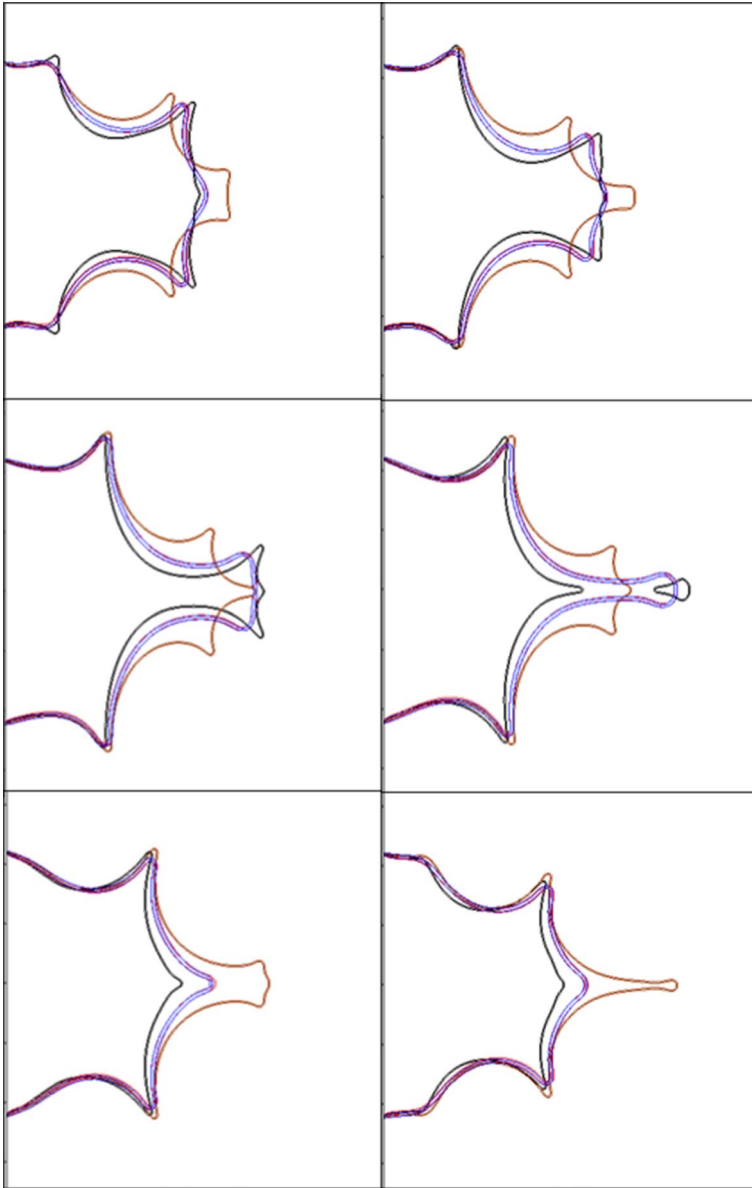


Fig. 14 Instantaneous flame positions during one entire acoustic forcing cycle. DNS (black), MATF on a fine mesh (blue), MATF on a course mesh (red) and NM on a course mesh (brown) are superposed

The breakout frame zooms in on a region upstream of the tip zone to highlight that CATF impairs flame wrinkling compared to the sharp folds observed in DNS and even MATF. Further deteriorating upon convection up the shear layer, the folds are unable to influence the flame tip in the same way resulting in the obvious displacement but also

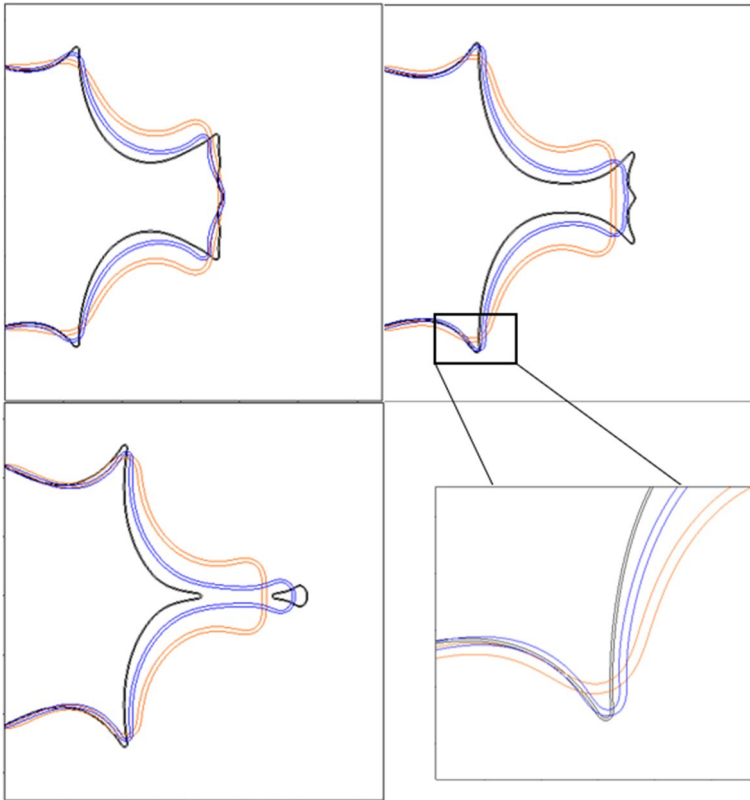


Fig. 15 Flame shapes during acoustic cycle. Comparison between DNS (black), MATF (blue) and CATF (orange)

wider and flatter flame pattern. Overall CATF results are very similar to Auzillon et al. (2011), with significant improvement in flame patterns with MATF.

Figure 16 plots the total heat release normalised by the mean, against time normalised by the acoustic period after initial transients have already faded. MATF shows excellent agreement with the peaks across most of the cycles and temporal thickening does not seem to have influenced period structure noticeably. There is some cycle-to-cycle variation observed even in the DNS but the net differences are small and model differences are maintained with CATF peak heat release lagging behind DNS and MATF.

The NM (not shown) fails to reproduce expected behaviour and undershoots peak heat release by up to 15%. Figure 16 illustrates how CATF still performs poorer than MATF as evident by overshooting of the troughs, likely due to obstructed surface annihilation as the wrinkled folds coalesce at the tip. In general the peaks for MATF are in better agreement with DNS in terms of magnitude. More noticeable is that CATF exhibits obvious changes in the slope close to the peak. Although not as pronounced as with NM there is a stark reduction in slope observed prior to max heat release, likely stemming from impaired pocket formation while MATF manages to better retain a more pronounced and sharp transition. Furthermore the latter also shows improvements in

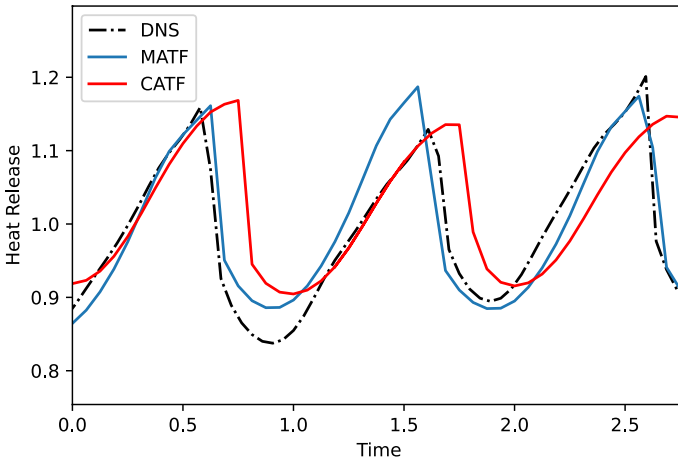


Fig. 16 Integrated heat release in the domain during acoustic forcing. Comparison between modified ATF (MATF) and classical ATF (CATF)

temporal behaviour by maintaining a reasonably accurate period cycle while classical ATF seems to lag behind and have a slightly longer period duration.

3.3 Turbulent Bunsen Flame

A lean, perfectly premixed methane-air mixture at equivalence ratio 0.7 is issued from an axisymmetric Bunsen type burner into a computational domain of $100 \times 50 \times 50$ mm as shown in Fig. 17. The burner itself has an inner diameter of 11.2 mm and feeds a reactant mixture at 300 K into the system with a velocity of 15.58 m/s. Turbulence is artificially generated using the method of Klein et al. (2003) and superimposed at the inlet with characteristic parameters from experiments, see Table 2, in terms of the integral, Taylor micro and Kolomogorov length scales (Λ_T , λ_T and η_K respectively). A classical Smagorinsky closure is adopted for SGS terms away from the flame with a Smagorinsky constant of 0.1.

The parameters corresponds to Case M14 in the full data matrix of Yuen and Gülder (2009) and is one of the most turbulent configurations considered. The resultant flame lies in the thin reaction zone of the turbulent combustion diagram with a turbulent Reynolds number of 324. The Damköhler and Karlovitz numbers are 1.2 and 13.4, suggesting significant impact of turbulence on the flame.

Four different simulations were run and are summarised in Table 3 with the sensor referring to either the symmetric implementation of Durand and Polifke (2007) or the asymmetric formulation developed as part of this work (see Sect. 2.3). The filter width is identified in terms of the level of refinement with the equivalent mesh resolution

Table 2 Turbulence characteristics for lean methane-air Bunsen flame *Source: Yuen and Gülder (2009)*

| Λ_T (mm) | λ_T (mm) | η_K (mm) | δ_f^0 (mm) | s_t^0 (m/s) | u'/s_t^0 | Λ/δ_f^0 |
|------------------|------------------|---------------|-------------------|---------------|------------|----------------------|
| 1.79 | 0.46 | 0.03 | 0.11 | 0.201 | 14.4 | 16.64 |

Fig. 17 Domain configuration for lean Bunsen flame. Flame surface iso-contours shown in red are encapsulated by AMR boxes at the finest level at all times. With blue arrows indicating the co-flow of hot products surrounding the central region

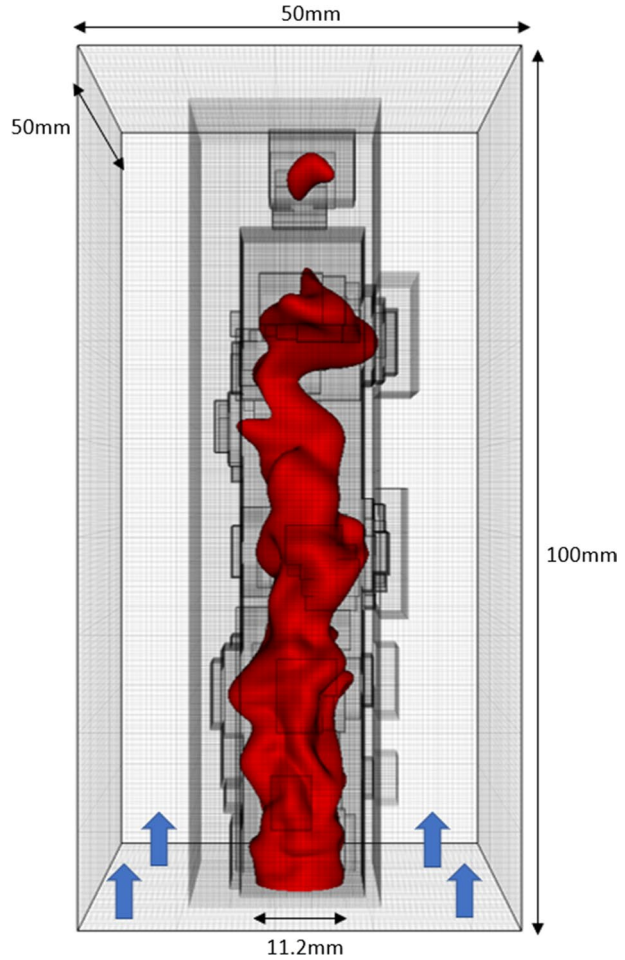


Table 3 Simulation parameters for lean premixed methane-air Bunsen flame

| Case | Mesh | Sensor | Filter width |
|------|--------|------------|--------------|
| A | Coarse | Symmetric | Level 1 |
| B | Coarse | Asymmetric | Level 1 |
| C | Coarse | Asymmetric | Level 2 |
| D | Fine | Asymmetric | Level 1 |

(Level 1/2). Two different meshes were used, both with three levels of refinement coupled with heuristically tuned tagging conditions on sharp variations in density. The mesh “regrids” every 100 time steps ensuring the flame front is always resolved on the finest level.

Table 4 shows mesh sizes in the coarsest and finest level, with approximate values for how many points lie within the thickened flame when using the thickening factor of $\mathcal{F} = 5$ employed in all simulations. Despite the moniker of “fine” both meshes are

Table 4 AMR grid spacing at coarsest/finest levels (i.e. Levels 1/3 respectively) and approximate flame resolution

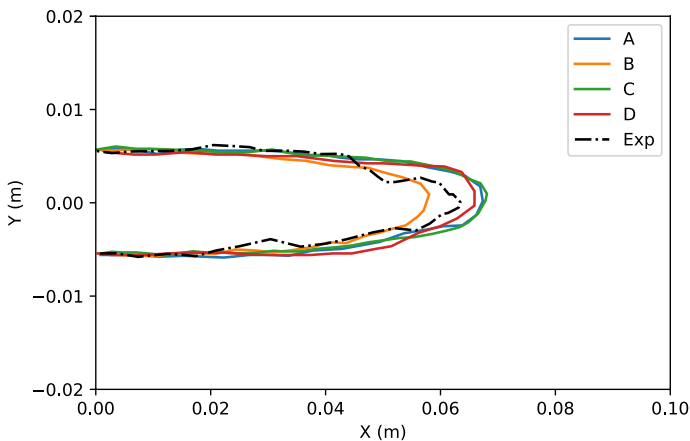
| Mesh | Level 1 [mm] | Level 3 [mm] | δ_f^0/Δ_3 | $\hat{\delta}_f^0/\Delta_3$ |
|--------|--------------|--------------|-----------------------|-----------------------------|
| Coarse | 0.69 | 0.17 | ~ 1 | ~ 4 |
| Fine | 0.35 | 0.08 | ~ 2 | ~ 8 |

significantly below the threshold of DNS with the coarse mesh having a grid spacing of the order of laminar flame thickness or even slightly larger.

Figure 18 illustrates time averaged profiles for a progress variable contour of 0.5 for simulations and the experimental counterpart. All approaches used here show excellent agreement and reliably reproduce global flame behaviour. Although some small differences are observed, they can be attributed to the thickening potentially displacing a particular contour in space within the larger flame zone. Even the coarser mesh simulations capture the overall quasi-steady state very well and this holds true even when the original grid resolution does not fully resolve the internal flame structure.

Figure 19 contains the same time averaged profiles for a variety of alternative modelling approaches sourced from literature such as a FSD based approach (C-FSD) and presumed conditional moment (PCM) with flame prolongation of intrinsic low-dimensional manifolds (FPI). Moreover included is the conventional thickened flame model with a power law efficiency function and thickening factor value of $\mathcal{F} = 3$ (labelled TF3). Care is warranted in making strict comparisons with reported simulations as they employed a different numerical discretisation. However, the present MATF simulations seems to outperform many of its alternatives in predicting global flame behaviour.

The curvature distribution is compared between MATF and reported data in Figs. 20 and 21 respectively. It is observed in the latter that filtering leads to a narrower peak by removing the small scale structures that lead to wrinkling with large curvature. Furthermore TF3 shows the narrowest peak, indicative of impaired turbulence-induced flame wrinkling. Despite the differences in numerical methods and uncertainties in post processing methods, which prevents a strict comparison, Fig. 20 suggest a marked improvement with MATF with less destruction of small scales.

**Fig. 18** Time averaged distribution of progress variable iso-contour of 0.5 for MATF. Experiment sourced from Hernández-Pérez et al. (2011)

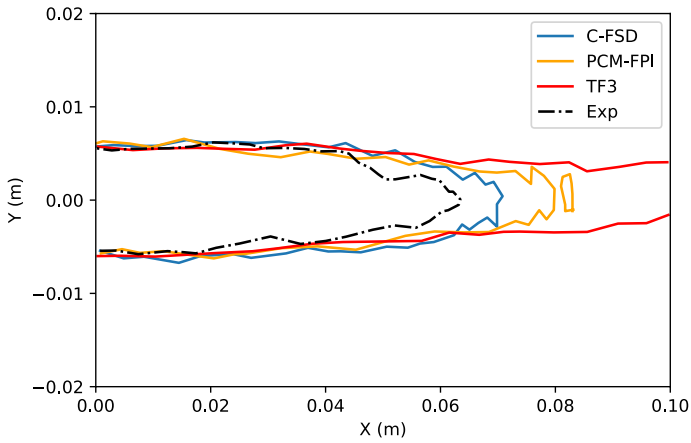


Fig. 19 Time averaged distribution of progress variable iso-contour of 0.5 for conventional LES methodologies. Adapted from Hernández-Pérez et al. (2011)

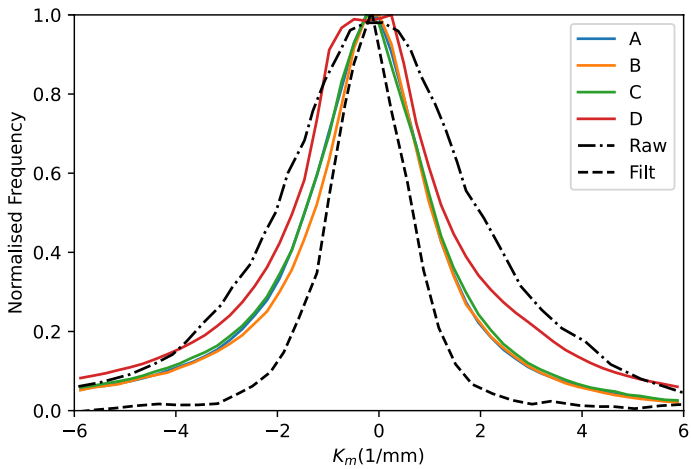


Fig. 20 Curvature distribution using MATF. Raw and filtered values sourced from Hernández-Pérez et al. (2011)

All three Cases A, B and C show very close agreement, suggesting that parameters such as choice of sensor or explicit AMR filter width have little effect on the curvature distribution. With the largest change being the result of improved grid resolution with Case D, which is still a fraction of the cost of conventional DNS (see Table 4) but close to approximate the experimental distribution.

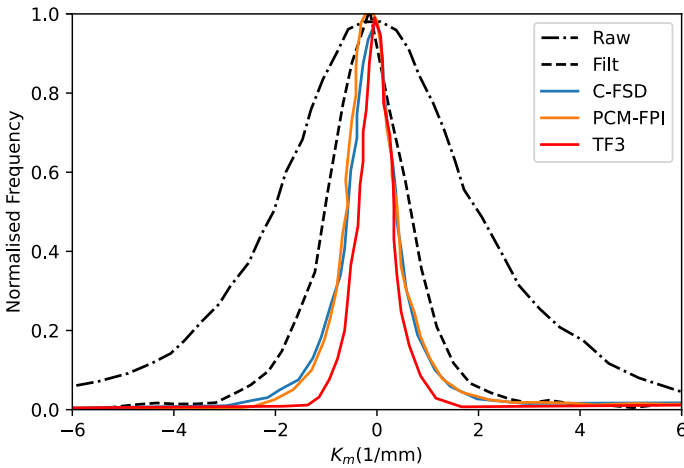


Fig. 21 Curvature distributions using conventional LES methodologies. Adapted from Hernández-Pérez et al. (2011)

4 Conclusion

Overall, the modified thickened flame model was shown to resolve (moderate) wrinkling well even without the use of an efficiency function for a series of canonical configurations. For large thickening factors, ATF methods face challenges with multi-step chemical pathways that is often overlooked in literature. However for a range of thickening factors with considerable relevance, the approach in conjunction with a suitable sensor yields good results.

Even for cases with significant movement of the flame such as when under acoustic modulations, flame dynamics are well replicated. The convection of an instability in flame surface through an active shear layer extends the range of applicability to include advection dominated flows. The modified model achieves grid independence with coarser meshes in contrast to the no-model approach.

The efficiency function is, by design, constructed to represent turbulence effects at smaller scales than the grid scales. The same is not necessarily true for the current approach as fluid scales smaller than Δ/\mathcal{F} will not be transformed. In practise this means a limitation to moderate Karlovitz numbers or alternatively finer meshes compared to conventional ATF. Similarly, close to the surface the new approach may not represent the flame-wall interaction correctly as the boundary layer may locally thicken. Nevertheless, the resultant framework was shown to perform well in predicting mean flame behaviour even when the internal structure is not well resolved without the need of an efficiency function.

The approach is well suited to benefit from AMR since there is no dependence on filter width close to the flame and no additional corrections, a priori, are required. The methodology holds promise either as a potential bridge between DNS and LES in terms of cost or in the form of hybrid models that can be extended to include efficiency functions (with high Karlovitz) or more complex sub-grid turbulence models.

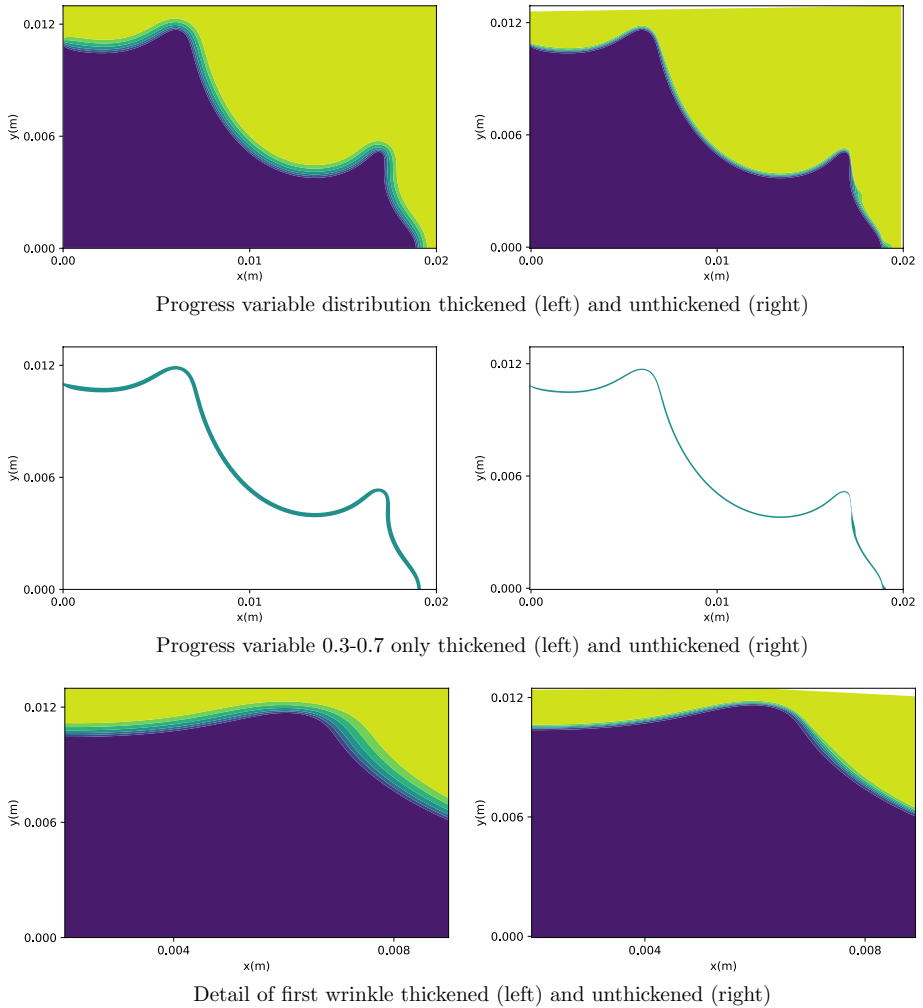


Fig. 22 Illustration of the reverse transform technique from a thickened to unthickened solution shown using different views of the progress variable

Appendix A: Reverse Transformation

All the contour plots in the paper show the thickened state, that result in flame structures that intuitively may seem larger, or perhaps cause spatial displacement of particular isocontours which could make direct comparison with experiments somewhat difficult.

As such it would be convenient if an unthickened state could be extracted from a thickened simulation. This can be done as a post processing technique by inverting the transformation presented in Sect. 2.2 to go from $\xi \rightarrow x$ instead as follows:

$$dx = \frac{d\xi}{\mathcal{F}(\xi, \eta)} \rightarrow x = x_0 + \int_{\xi_0}^{\xi} \frac{d\xi}{\mathcal{F}(\xi, \eta)} \quad (\text{A1})$$

$$dy = \frac{d\eta}{\mathcal{F}(\xi, \eta)} \rightarrow y = y_0 + \int_{\eta_0}^{\eta} \frac{d\eta}{\mathcal{F}(\xi, \eta)} \quad (\text{A2})$$

In general, \mathcal{F} is a function of space when using a sensor and cannot be pulled out of the integral. Therefore the integral is solved numerically via Eqs. (A3) and (A4) to obtain an unthickened coordinate system. Where the j -index refers to a sequential loop over all elements in the mesh and \mathcal{F}_j between two points can be approximated by a simple linear interpolation if the variation is smooth enough.

$$x_k = x_0 + \sum_{j=1}^k \frac{\xi_j - \xi_{j-1}}{\mathcal{F}_j} \quad (\text{A3})$$

$$y_k = y_0 + \sum_{j=1}^k \frac{\eta_j - \eta_{j-1}}{\mathcal{F}_j} \quad (\text{A4})$$

The procedure is simple, cheap, can be done a posteriori and offers several unique benefits. Figure 22 illustrates the process on a slice from the acoustic flame simulation where a thickening factor of 4 was used. The top row shows the complete domain profile of progress variable and it can be seen that the transformation results in a close resemblance to actual flame resolved simulations. The second row contains a solid band representing the core of the flame zone and demonstrates how the procedure essentially shrinks the reactive zone based on the local sensor value which collapses the spatial solution uniformly to a more compressed state. Similarly this point is further made clear by a close up of the distorted flame surface in the final row where progress variable contours are seen to cluster together post reverse-transform. Such a direct reverse transform is only possible because *all* scales are transformed. The use of an efficiency function formulation would require additional corrections.

Acknowledgements The authors would like to acknowledge UKCTRF for providing the computational access to the ARCHER UK National Supercomputing Service.

Author Contributions OR and SNM contributed to the conception of the presented idea. OR wrote the main text, performed the numerical simulations and prepared all figures. SNM revised the manuscript. All authors reviewed the manuscript.

Funding This work has been funded by EPSRC-DTP Programme.

Declarations

Conflict of interest The authors have no conflict of interests to declare that are relevant to the content of this article.

Ethics Approval Not applicable.

Informed Consent Not applicable.

Open Access This article is licensed under a Creative Commons Attribution 4.0 International License, which permits use, sharing, adaptation, distribution and reproduction in any medium or format, as long as you give appropriate credit to the original author(s) and the source, provide a link to the Creative Commons licence, and indicate if changes were made. The images or other third party material in this article are included in the article's Creative Commons licence, unless indicated otherwise in a credit line to the material. If material is not included in the article's Creative Commons licence and your intended use is not permitted by statutory regulation or exceeds the permitted use, you will need to obtain permission directly from the copyright holder. To view a copy of this licence, visit <http://creativecommons.org/licenses/by/4.0/>.

References

- Almeida, Y.P., Navarro-Martinez, S.: Large eddy simulation of a supersonic lifted flame using the Eulerian stochastic fields method. *Proc. Combust. Inst.* **37**(3), 3693–3701 (2019)
- Auzillon, P., Fiorina, B., Vicquelin, R., et al.: Modeling chemical flame structure and combustion dynamics in les. *Proc. Combust. Inst.* **33**(1), 1331–1338 (2011)
- Bell, J., Almgren, A., Beckner, V., et al.: Boxlib user's guide. github.com/BoxLib-Codes/BoxLib (2012)
- Bénard, P., Lartigue, G., Moureau, V., et al.: Large-eddy simulation of the lean-premixed preceinsta burner with wall heat loss. *Proc. Combust. Inst.* **37**(4), 5233–5243 (2019)
- Butler, T., O'Rourke, P.: A numerical method for two dimensional unsteady reacting flows. In: Symposium (international) on combustion, pp. 1503–1515 (1977)
- Charlette, F., Meneveau, C., Veynante, D.: A power-law flame wrinkling model for les of premixed turbulent combustion part i: non-dynamic formulation and initial tests. *Combust. Flame* **131**(1–2), 159–180 (2002)
- Chow, F.K., Moin, P.: A further study of numerical errors in large-eddy simulations. *J. Comput. Phys.* **184**(2), 366–380 (2003)
- Colin, O., Ducros, F., Veynante, D., et al.: A thickened flame model for large eddy simulations of turbulent premixed combustion. *Phys. Fluids* **12**(7), 1843–1863 (2000)
- Cuenot, B., Shum-Kivan, F., Blanchard, S.: The thickened flame approach for non-premixed combustion: Principles and implications for turbulent combustion modeling. *Combust. Flame* **239**, 111702 (2022)
- De, A., Acharya, S.: Large eddy simulation of a premixed Bunsen flame using a modified thickened-flame model at two Reynolds number. *Combust. Sci. Technol.* **181**(10), 1231–1272 (2009)
- Domingo, P., Vervisch, L., Payet, S., et al.: Dns of a premixed turbulent v flame and les of a ducted flame using a fsd-pdf subgrid scale closure with fpi-tabulated chemistry. *Combust. Flame* **143**(4), 566–586 (2005)
- Ducros, F., Ferrand, V., Nicoud, F., et al.: Large-eddy simulation of the shock/turbulence interaction. *J. Comput. Phys.* **152**(2), 517–549 (1999)
- Ducros, F., Laporte, F., Soulères, T., et al.: High-order fluxes for conservative skew-symmetric-like schemes in structured meshes: application to compressible flows. *J. Comput. Phys.* **161**(1), 114–139 (2000)
- Ducruix, S., Durox, D., Candel, S.: Theoretical and experimental determinations of the transfer function of a laminar premixed flame. *Proc. Combust. Inst.* **28**(1), 765–773 (2000)
- Durand, L., Polifke, W.: Implementation of the thickened flame model for large eddy simulation of turbulent premixed combustion in a commercial solver. In: ASME Turbo Expo 2007: Power for Land, Sea, and Air, pp. 869–878 (2007)
- Durox, D., Schuller, T., Candel, S.: Combustion dynamics of inverted conical flames. *Proc. Combust. Inst.* **30**(2), 1717–1724 (2005)
- Durox, D., Schuller, T., Noiray, N., et al.: Experimental analysis of nonlinear flame transfer functions for different flame geometries. *Proc. Combust. Inst.* **32**(1), 1391–1398 (2009)
- Emami, S., Mazaheri, K., Shamooni, A., et al.: Les of flame acceleration and ddt in hydrogen-air mixture using artificially thickened flame approach and detailed chemical kinetics. *Int. J. Hydrog. Energy* **40**(23), 7395–7408 (2015)
- Franzelli, B., Riber, E., Sanjosé, M., et al.: A two-step chemical scheme for kerosene-air premixed flames. *Combust. Flame* **157**(7), 1364–1373 (2010)
- Freitag, M., Klein, M.: An improved method to assess the quality of large eddy simulations in the context of implicit filtering. *J. Turbul.* **7**, N40 (2006)
- Fureby, C.: Large eddy simulation modelling of combustion for propulsion applications. *Philos. Trans. R. Soc. A Math. Phys. Eng. Sci.* **367**(1899), 2957–2969 (2009)

- Geurts, B.J., Fröhlich, J.: A framework for predicting accuracy limitations in large-eddy simulation. *Phys. Fluids* **14**(6), L41–L44 (2002)
- Gicquel, L.Y., Staffelbach, G., Poinso, T.: Large eddy simulations of gaseous flames in gas turbine combustion chambers. *Prog. Energy Combust. Sci.* **38**(6), 782–817 (2012)
- Hawkes, E.R., Cant, R.: A flame surface density approach to large-eddy simulation of premixed turbulent combustion. *Proc. Combust. Inst.* **28**(1), 51–58 (2000)
- Hernández-Pérez, F., Yuen, F., Groth, C., et al.: Les of a laboratory-scale turbulent premixed Bunsen flame using fsd, pcm-fpi and thickened flame models. *Proc. Combust. Inst.* **33**(1), 1365–1371 (2011)
- Kazmouz, S.J., Haworth, D.C., Lillo, P., et al.: Extension of a thickened flame model to highly stratified combustion-application to a spark-ignition engine. *Combust. Flame* **236**(111), 798 (2022)
- Klein, M., Sadiki, A., Janicka, J.: A digital filter based generation of inflow data for spatially developing direct numerical or large eddy simulations. *J. Comput. Phys.* **186**(2), 652–665 (2003)
- Kraus, C., Selle, L., Poinso, T.: Coupling heat transfer and large eddy simulation for combustion instability prediction in a swirl burner. *Combust. Flame* **191**, 239–251 (2018)
- Kuenne, G., Ketelheun, A., Janicka, J.: LES modeling of premixed combustion using a thickened flame approach coupled with FGM tabulated chemistry. *Combust. Flame* **158**(9), 1750–1767 (2011)
- Kuhlmann, J., Lampmann, A., Pfitzner, M., et al.: Assessing accuracy, reliability and efficiency of combustion models for prediction of flame dynamics with large eddy simulation. *Phys. Fluids* **34**(9), 095–117 (2022)
- Kuo, K.K.: Principles of combustion. Elsevier Science Pub. Co., Inc., New York, NY (1986)
- Légier, J., Poinso, T., Varoquié, B., et al.: Large eddy simulation of a non-premixed turbulent burner using a dynamically thickened flame model. In: IUTAM Symposium on Turbulent Mixing and Combustion, Springer, pp. 315–326 (2002)
- Lodato G (2008) Tridimensional boundary conditions for direct and large-eddy simulation of turbulent flows. sub-grid scale modeling for near-wall region turbulence. PhD thesis, INSA de Rouen
- Louch, D., Bray, K.: Vorticity in unsteady premixed flames: vortex pair-premixed flame interactions under imposed body forces and various degrees of heat release and laminar flame thickness. *Combust. Flame* **125**(4), 1279–1309 (2001)
- Maio, G., Cailler, M., Mercier, R., et al.: Virtual chemistry for temperature and co prediction in les of non-adiabatic turbulent flames. *Proc. Combust. Inst.* **37**(2), 2591–2599 (2019)
- McMurtry, P., Riley, J.J., Metcalfe, R.: Effects of heat release on the large-scale structure in turbulent mixing layers. *J. Fluid Mech.* **199**, 297–332 (1989)
- McMurtry, P.A., Jou, W.H., Riley, J., et al.: Direct numerical simulations of a reacting mixing layer with chemical heat release. *AIAA J.* **24**(6), 962–970 (1986)
- Mehl, C., Liu, S., Colin, O.: A strategy to couple thickened flame model and adaptive mesh refinement for the les of turbulent premixed combustion. *Flow Turbul. Combust.* **107**(4), 1003–1034 (2021)
- Peters, N.: Turbulent combustion. Cambridge University Press, Cambridge (2001)
- Picciani, M., Richardson, E., Navarro-Martinez, S.: Resolution requirements in stochastic field simulation of turbulent premixed flames. *Flow Turbul. Combust.* **101**(4), 1103–1118 (2018)
- Picciani, M., Richardson, E., Navarro-Martinez, S.: A thickened stochastic fields approach for turbulent combustion simulation. *Flow Turbul. Combust.* **101**(4), 1119–1136 (2018)
- Pirozzoli, S.: Numerical methods for high-speed flows. *Annu. Rev. Fluid Mech.* **43**, 163–194 (2011)
- Pitsch, H.: Large-eddy simulation of turbulent combustion. *Annu. Rev. Fluid Mech.* **38**, 453–482 (2006)
- Pitsch, H., Duchamp de Lageneste, L.: Large-eddy simulation of premixed turbulent combustion using a level-set approach. *Proc. Combust. Inst.* **29**(2), 2001–2008 (2002)
- Poinso, T., Veynante, D., Candel, S.: Quenching processes and premixed turbulent combustion diagrams. *J. Fluid Mech.* **228**, 561–606 (1991)
- Poinso, T.J., Lele, S.: Boundary conditions for direct simulations of compressible viscous flows. *J. Comput. Phys.* **101**(1), 104–129 (1992)
- Pope, S.B.: Ten questions concerning the large-eddy simulation of turbulent flows. *New J. Phys.* **6**(1), 35 (2004)
- Popp, S., Kuenne, G., Janicka, J., et al.: An extended artificial thickening approach for strained premixed flames. *Combust. Flame* **206**, 252–265 (2019)
- Proch, F., Kempf, A.M.: Numerical analysis of the Cambridge stratified flame series using artificial thickened flame les with tabulated premixed flame chemistry. *Combust. Flame* **161**(10), 2627–2646 (2014)
- Rochette, B., Collin-Bastiani, F., Gicquel, L., et al.: Influence of chemical schemes, numerical method and dynamic turbulent combustion modeling on les of premixed turbulent flames. *Combust. Flame* **191**, 417–430 (2018)
- Rochette, B., Riber, E., Cuenot, B., et al.: A generic and self-adapting method for flame detection and thickening in the thickened flame model. *Combust. Flame* **212**, 448–458 (2020)

- Schuller, T., Ducruix, S., Durox, D., et al.: Modeling tools for the prediction of premixed flame transfer functions. *Proc. Combust. Inst.* **29**(1), 107–113 (2002)
- Strakey, P.A., Eggenspieler, G.: Development and validation of a thickened flame modeling approach for large eddy simulation of premixed combustion. *ASME. J. Eng. Gas Turbines Power* **132**(7), 071501 (2010). <https://doi.org/10.1115/1.4000119>
- Straub, C., Kronenburg, A., Stein, O.T., et al.: Multiple mapping conditioning coupled with an artificially thickened flame model for turbulent premixed combustion. *Combust. Flame* **196**, 325–336 (2018)
- Thibaut, D., Candel, S.: Numerical study of unsteady turbulent premixed combustion: Application to flashback simulation. *Combust. Flame* **113**(1–2), 53–65 (1998)
- Van Oijen, J., De Goey, L.: Modelling of premixed laminar flames using flamelet-generated manifolds. *Combust. Sci. Technol.* **161**(1), 113–137 (2000)
- Vermorel, O., Quillatre, P., Poinot, T.: LES of explosions in venting chamber: A test case for premixed turbulent combustion models. *Combust. Flame* **183**, 207–223 (2017)
- Wang, G., Boileau, M., Veynante, D.: Implementation of a dynamic thickened flame model for large eddy simulations of turbulent premixed combustion. *Combust. Flame* **158**(11), 2199–2213 (2011)
- Williams, F.A.: *Combustion theory*. CRC Press, Boca Raton (2018)
- Yetter, R., Dryer, F., Rabitz, H.: A comprehensive reaction mechanism for carbon monoxide/hydrogen/oxygen kinetics. *Combust. Sci. Technol.* **79**(1–3), 97–128 (1991)
- Yu, S., Navarro-Martinez, S.: Modelling of deflagration to detonation transition using flame thickening. *Proc. Combust. Inst.* **35**(2), 1955–1961 (2015)
- Yuen, F.T., Gülder, Ö.L.: Premixed turbulent flame front structure investigation by Rayleigh scattering in the thin reaction zone regime. *Proc. Combust. Inst.* **32**(2), 1747–1754 (2009)
- Zhang, P., Park, J.W., Wu, B., et al.: Large eddy simulation/thickened flame model simulations of a lean partially premixed gas turbine model combustor. *Combust. Theor. Model.* **25**(7), 1296–1323 (2021)

Publisher's Note Springer Nature remains neutral with regard to jurisdictional claims in published maps and institutional affiliations.